GSA Data Repository 2016330

***Comparison between simulated and observed present-day precipitation, temperature, and isotopic compositions of precipitation ($\delta^{18}O_p$) and soil water ($\delta^{18}O_{sw}$) across the western North America***

Simulation skill of the ECHAM5-JSBACH-wiso model is evaluated by comparing simulated present-day temperature and precipitation to observational data of Modern Era Retrospective-analysis for Research and Applications (MERRA) (Rienecker et al., 2011) (Figs. DR1A-C). The simulations reach equilibrium in the first 5 years and have no discernable trend in the following 15 model years. Model results are therefore averaged over this period. MERRA data are annual averages over the period of 1979 to 2011. Simulated spatial distributions, including the meridional gradients and east-west contrast of temperature and precipitation between the western Cordillera and central Great plain are broadly consistent with observations. The model underestimates topographic gradients of temperature and precipitation across local-scale reliefs of the western Cordillera. This bias is mostly related to the model resolution: the surface elevation of each grid cell is averaged over the related grid area (~200 $km^2$) in the model, which does not preserve the topographic gradient across reliefs and basins.

Model simulations of broad-scale continental $\delta^{18}O_p$ gradients between the Great Basin and its surrounding mountains match observations (Fig. DR2A). Limited by resolution, local variability of $\delta^{18}O_p$ is underestimated. Simulated present-day $\delta^{18}O$ of soil water ($\delta^{18}O_{sw}$) (2.1 ‰) is close to the derived $\delta^{18}O_{sw}$ below 50cm depth at central New Mexico sites (~34 °N, 106 °W) with shrubland biome type (1.2 – 1.6 ‰) (Great Basin Shrubland and Chihuahuan Shrubland). Simulated $\delta^{18}O_{sw}$ is more enriched (~2 ‰) than the measured $\delta^{18}O_{sw}$ at Pinon-Juniper woodland site (-6.4 ‰) (Breecker et al., 2009). The $\delta^{18}O_{sw}$ mismatch at this site may reflect local

interannual climate variability that is not represented in the model results. Anomalous amount of winter snowfall occurred in central New Mexico during the measurement time of 2006 – 2007 (Breecker et al., 2009). The soil water pool around Pinon-Juniper site may have stored higher percentage of snowmelt water than the other sites, resulting in $^{18}O$-depleted soil water.

***Experiment setup***

ECHAM5-JSBACH-wiso experiments are conducted to explore climatic and isotopic responses across the western U.S. to four major aspects of Neogene environmental changes, including 1) intensification of equator-to-pole temperature gradient, and 2) strengthening of tropical Pacific zonal SST gradient, 3) grassland expansion and 4) geographic and topographic changes (Table DR 1). In all experiments, the longitudinal width of the Great Basin is kept the same. The Neogene extension of Great Basin may contribute to its lateral growth of ~235 km (McQuarrie and Wernicke, 2005). The $\delta^{18}O_{sw}$ responses to such an extension can be estimated applying the isotopic gradient along the airflow trajectory from the Gulf of Mexico (black line in Fig. DR2A). This gradient is ~0.005 ‰/km, suggesting a ~1.2 ‰ potential enrichment due to basin extension. This effect is relatively small in comparison to recorded changes by Neogene $\delta^{18}O$ records and therefore, not considered in our simulations.

Details of the boundary conditions of the different ECHAM5-JSBACH-wiso experiments are discussed in the following and summarized in Table DR1. Corresponding maps of boundary conditions are shown in Fig. DR3.

1) NG-EPGRAD. The shrunken high-latitude glacier extend, low meridional SST gradient (Figs. DR3A and DR3D) and higher $CO_2$ level all contribute to a low equator-to-pole temperature gradient during the early-to-middle Miocene (Goldner et al., 2014). The Mid-Miocene SST is modified from results of an atmosphere-ocean coupled simulation of Mid-

Miocene climate by Herold et al., (2011, 2012). This simulation features a much steeper meridional SST gradient than reconstructed (see a compilation by Goldner et al., (2014)) with near modern values in the tropics and freezing polar SSTs (-1.8 °C). Given that our focus is to look at the regional climate and isotopic responses to Neogene changes in equator-to-pole SST gradient, it is important to represent this gradient correctly in the model. Therefore, the SST gradient in Herold et al, (2011, 2012) is adjusted to represent the Mid-Miocene reconstructions. A zonally uniform adjusting factor is added to each latitudes of the SST data: $\Delta SST = \sin\left(\left|\frac{SST_{mean-20}-20}{44}\right| \times \pi\right) \times 7$, $SST_{mean\text{-}20}$ is the zonal SST average (°C) with SSTs warmer than 20 °C set to 20 °C. ΔSST=0 for regions with zonal mean SSTs ≥ 20 °C, ΔSST=~7°C for polar SSTs. The resulted ~5°C SST at the poles is close to the median of the proxy reconstructions (Fig. 1a in Goldner et al., 2014). Accordingly, simulated sea ice in Herold et al., (2011, 2012) is set to zeros at grid cells where the adjusted SSTs are above -1.8 °C. A 3-point smoothing is then applied to sea ice monthly cycle to eliminate sharp monthly sea ice transitions.

2) NG-ELNINO. We use SST anomalies of the 1997-1998 El Niño event to construct an El Niño SST pattern, featuring reduced tropical Pacific zonal SST gradient (Fig. DR3E). The choice of this El Niño event is based on Molnar and Cane (2007), which suggests that terrestrial reconstructions of early Pliocene temperature and precipitation reflect an El Niño pattern most similar to the 1997-1998 event. The SST anomalies are calculated as departures of mean annual SSTs during the event between April 1997 to March 1998 from 30-yr climatology using NOAA ERSST.v3 (Smith and Reynolds, 2004).

3) NG-GRASS. We infer forest biomes at places that are currently covered by grassland using nearest neighborhood extrapolation, i.e. for each cell, if the dominant vegetation cover is

grassland, vegetation related variables are replaced with values from the nearest cells with considerable (≥ 40%) forest coverage (Figs. DR3C and DR3G).

4) NG-GEO. The Mid-Miocene reconstructions of coastal line and topographic configurations (Herold et al., 2008) outside the North America are applied to test climatic and isotopic responses to global-scale geographic and topographic reconfiguration (Figs. DR3B and DR3F). In order to minimize the associated changes in vegetation cover, uniform global mean present-day vegetation is prescribed for the Mid-Miocene case. An additional experiment with the same vegetation distribution and present-day geography and topography is performed to serve as the control for this case.

***Comparison with Neogene changes in precipitation recorded by proxy records***

In the western U.S., where fossil flora and paleosol records indicate the greatest Neogene aridification, annual precipitation amounts are inferred to have decreased by ~75 - 814 mm/yr (from 12 – 18 Ma to present) (Table DR4). The precipitation reduction displays a northwest-to-southeast trend with greatest reduction in western central Idaho (750-877 mm/yr) and smallest reduction in northern Texas (124-275 mm/yr). Among our four sensitivity tests, only an increase in equator-to-pole gradient yields a response that is consistent with the proxy records. The precipitation response can explain over one-half of the decrease in precipitation (3 – 497.5 mm/yr reduction at proxy sites) and resembles the northwest-southeast pattern of precipitation reduction indicated by proxies (Fig. DR5A). Simulated precipitation responses to the other Neogene environmental factors are inconsistent with the proxy data in magnitude (Fig. DR5C), sign (Fig. DR5D), and/or spatial distribution (Fig. DR5B-D).

***Comparison with Grassland Hypothesis: Neogene $\delta^{18}O$ enrichment across the western U.S. is due to grassland expansion***

Replacing forests with grassland was proposed to increase the evapotranspiration to precipitation (E-P) ratio, which damps $^{18}O$ rainout and increases precipitation $\delta^{18}O$ due to enhanced water recycling. However, differences in evapotranspiration ratios used by previous studies (Mix et al. 2013; Chamberlain et al., 2014) are attributable to both plant physiological differences (grassland versus forests), and climatic differences between observational sites (Colorado versus North Carolina). The latter difference is not accounted for previously. Solely attributing differences of evapotranspiration ratios to plant physiological differences leads to overestimates of $\delta^{18}O$ changes. Additionally, we simulate strong climate responses to grassland expansion that counteract the potential enrichment effect due to increasing evapotranspiration ratio. Grassland expansion leads to significant cooling (~2 °C) and an increase in snowfall (up to 40% increase) in our simulations (Fig. DR6), both of which contribute to a decrease in $\delta^{18}O_{sw}$. The shallow rooting depth of grasses compared to trees also contributes to a $\boldsymbol{\delta}^{18}O$ increase of ~2 ‰ (Mix et al., 2013). This effect is not included in the model, but is likely small given its dependence on responses of evapotranspiration ratio, which only shows a slight increase (~10 %) in the model by replacing forests with grassland across the western U.S.

***Local $\Delta\delta^{18}O_{elev}$ variability***

We subtract the mineral $\delta^{18}O$ ($\delta^{18}O_m$) responses to Neogene strengthening of the equator-to-pole temperature gradient ($\Delta\delta^{18}O_{epgrad}$) from proxy changes ($\Delta\delta^{18}O_m$) to isolate the elevation-dependent $\delta^{18}O$ signal ($\Delta\delta^{18}O_{elev} = \Delta\delta^{18}O_m - \Delta\delta^{18}O_{epgrad}$). The positive $\Delta\delta^{18}O_{elev}$ at proxy locations across Great Basin may reflect regional subsidence of this region during the Neogene. However, the negative $\Delta\delta^{18}O_{elev}$ in the northern Great Basin (Ibapah badland, Middle and North Park, and Hageman site in Fig. 2C) and strong positive $\Delta\delta^{18}O_{elev}$ in the El Paso Basin (11.4 ‰) of southern Sierra Nevada cannot be explained by an enhanced equator-to-pole gradient or

tectonic subsidence. The strong proxy enrichment in El Paso Basin likely reflects strong evaporation in a closed basin. The Sr/Ca ratio and covariance of $\delta^{13}C$ and $\delta^{18}O$ of carbonates indicate high-salinity lake water likely resulted from this process (Horton and Chamberlain, 2006). The small-scale topography of the El Paso Basin, and associated hydrological changes, however, are not resolved in the current model configuration. The same model limitation in representing subgrid scale topography and associated hydrological features may also explain the negative $\delta^{18}O_{elev}$ in the northern Great Basin and central Rockies. In our simulations, snowfall increases at high altitude sites across the Rockies and Northern Great Basin in response to a greater equator-to-pole temperature gradient. Abundant snow-water discharge from surrounding regions of high relief could overwhelm the warm season $O^{18}$-enrichment at proxy sites located at intermountain basins, which, however, is not resolved in the model. Alternatively, depletion signals from these sites may record small amounts of local uplift, which are not represented in our simulations.

Table DR1. Key boundary conditions for testing isotopic responses to four major aspects of Neogene environmental changes.

| **Experiment** | **Neogene environmental change** | **Boundary conditions** |
|---|---|---|
| CNTL | None | Preindustrial $CO_2$ (280 ppm) and vegetation cover; present-day geography and topography; present-day trace gases and SST climatology (1979-2011) |
| NG-EPGRAD | Increasing equator-to-pole temperature gradient | 560 ppm $CO_2$, Mid-Miocene glacier coverage and SST pattern (Herold et al., 2011), equator-to-pole SST gradient adjusted to mimic proxy values (Goldner et al., 2014) |
| NG-ELNINO | Termination of El Niño-like SST state | El Niño SST pattern (estimated using SST anomalies of 1997-1998 El Niño event, based on Molnar and Cane, (2007) |
| NG-GRASS | Grassland expansion | Forested North America |
| NG-GEO | Geographic and topographic changes | Global average of modern vegetation cover, Mid-Miocene geography and topography with North America region restored to present-day geography and topography (Herold, et al., 2008) |

Table DR2 $^{18}O$ fractionation factors between soil water and different types of minerals used in the study.

| Mineral | Fractionation factor (α) | References |
|---|---|---|
| Calcite | $1000\ln\alpha_{calcite-water} = 2.78 \times 10^6 \times T^{-2} - 2.89$ | Friedman and O'Neil, 1977 |
| Volcanic glasses | $1000\ln\alpha_{glass-water} = 1/1.0343$ | Friedman, et al., 1993 |
| Smectite | $1000\ln\alpha_{smectite-water} = 2.55 \times 10^6 \times T^{-2} - 4.05$ | Sheppard and Gilg, 1996 |

Table DR3. Neogene proxy $\delta^{18}O$ trends across the western U.S.

| Latitude (Modern) | Longitude (Modern) | Proxy material | Significance Level | Trend (‰/10myrs) | Location |
|---|---|---|---|---|---|
| 44.9 | -111.9 | Pedogenic carbonate | 0.0038 | 1.4 | Montana Basins, MN[1] |
| 40.6 | -115.7 | Pedogenic carbonate | 0.0001 | 4.5 | Elko Basin,NV[1] |
| 42.8 | -115.2 | Pedogenic carbonate | 0.0000 | -4.0 | Hagerman, ID[1] |
| 40.6 | -106.4 | Pedogenic carbonate | 0.0002 | 1.0 | Middle and North Park, CO[1] |
| 40.1 | -114.1 | Pedogenic carbonate | 0.3355 | -6.3 | Ibapah Badlands, UT[1] |
| 36.4 | -117.8 | Pedogenic carbonate | 0.0217 | 3.9 | Fish Lake Valley, NV[2] |
| 42.0 | -103.4 | Glasses* | 0.0048 | 3.9 | Western Great Plain, NE[3] |
| 42.1 | -107.6 | Glasses* | 0.0028 | 2.9 | Central Rockies, WY[3] |
| 35.0 | -117.0 | Smectite* | 0.1854 | 1.0 | Rainbow Basin, CA[4] |
| 35.4 | -117.9 | smectite* | 0.0000 | 11.4 | El Paso Basin, CA[4] |
| 38.0 | -118.2 | smectite* | 0.0590 | 1.2 | Eastern Sierra Nevada, NV[5] |
| 41.8 | -114.6 | smectite* | 0.0024 | 2.7 | Northern Basin and Range, ID[6] |
| 41.3 | -102.3 | Pedogenic carbonate | 0.0040 | 3.3 | Nebraska Composite section, NE[2] |

* Trends of $\delta D$ are scaled to $\delta^{18}O$ by multiplying 1/8.


[1] Chamberlain, C. P., Mix, H. T., Mulch, A., Hren, M. T., Kent-Corson, M. L., Davis, S. J., et al., 2012. The Cenozoic climatic and topographic evolution of the western North American Cordillera. American Journal of Science, 312, 213–262. http://doi.org/10.2475/02.2012.05

[2] Mix, H. T., Winnick, M. J., Mulch, A., & Page Chamberlain, C., 2013. Grassland expansion as an instrument of hydrologic change in Neogene western North America. Earth and Planetary Science Letters, 377-378, 73–83. http://doi.org/10.1016/j.epsl.2013.07.032

[3] Fan, M., Heller, P., Allen, S. D., & Hough, B. G., 2014. Middle Cenozoic uplift and concomitant drying in the central Rocky Mountains and adjacent Great Plains. Geology, 42(6), 547–550. http://doi.org/10.1130/G35444.1

[4] Horton, T. W., & Chamberlain, C. P., 2006. Stable isotopic evidence for Neogene surface downdrop in the central Basin and Range Province. Geological Society of America Bulletin, 118(3-4), 475–490. http://doi.org/10.1130/B25808

[5] Poage, M. A., and Chamberlain, C. P., 2001. Stable isotopic evidence for a Pre□Middle Miocene rain shadow in the western Basin and Range: Implications for the paleotopography of the Sierra Nevada. Tectonics, 21(4). http://doi.org/10.1029/2001TC001303

[6] Horton, T. W., Sjostrom, D. J., Abruzzese, M. J., Poage, M. A., Waldbauer, J. R., Hren, M., et al., 2004. Spatial and temporal variation of Cenozoic surface elevation in the Great Basin and Sierra Nevada. American Journal of Science, 304(10), 862–888. http://doi.org/10.2475/ajs.304.10.862

Table DR4. Differences of present-day observations and reconstructed early-to-middle Miocene precipitation over the western U.S.

| lat (Modern) | lon (Modern) | Age (Ma) | Min (mm) | Max (mm) | Location | Modern (MERRA) | Modern minus Proxy (Min) | Modern minus Proxy (Max) |
|---|---|---|---|---|---|---|---|---|
| 36.3 | -121.4 | 17 | 653 | 760 | Carmel Valley[1] | 457.3 | -195.7 | -302.7 |
| 39 | -118.2 | 18.5 | 760 | 890 | Middlegate Basin[2] | 304.8 | -455.2 | -585.2 |
| 39 | -117.7 | 18 | 890 | 1000 | Buffalo Canyon[3] | 304.8 | -585.2 | -695.2 |
| 35.3 | -119.7 | 15 | 635 | 635 | Tembler California[4] | 213.3 | -421.7 | -421.7 |
| 44.8 | -114.7 | 16.0 - 15.4 | 700 | 700 | Picture Gorge Subgroup[5] | 555.3 | -144.7 | -144.7 |
| 42 | -114 | 9-11.8 | 1143 | 1270 | Trapper Creek Formation[6] | 392.2 | -750.8 | -877.8 |
| 35 | -101 | 10.-12. | 475 | 875 | Clarendon, TX[1] | 599.9 | 124.9 | -275.1 |
| 37 | -100 | 10.-12. | 550 | 950 | Beaver, Oklahoma[1] | 570.4 | 20.4 | -379.6 |
| 44.2 | -118 | ~12 | 623 | 879 | Ironside, Oregon[7] | 319.9 | -303.1 | -559.1 |

[1] Axelrod D. I., 1979. Desert vegetation, its age and origin. In: Goodin JR & DK Northington (eds). Arid Land Plant Resources: 1-72. International Center for Arid and Semi-arid Land Studies, Texas Tech University, Lubbock, Texas.
[2] Axelrod D. I., 1985. Miocene floras from the Middlegate basin, west-central Nevada. University of California Publications in Geological Sciences 129.
[3] Axelrod D. I., 1991. The Miocene Buffalo Canyon flora, western Nevada. University of California Publications in Geological Sciences 135.
[4] Axelrod D. I., 1995. The middle Miocene Purple Mountain flora of western Nevada: Univ. of California Publ. Geol. Sci., 139, 62 p.
[5] Sheldon, N. D., 2006. Using paleosols of the Picture Gorge Basalt to reconstruct the middle Miocene climatic optimum. PaleoBios, 26(2), 27-36.
[6] Leopold, E. B., and Denton, M. F., 1987. Comparative age of grassland and steppe east and west of the northern rocky mountain. Annals of the Missouri Botanical Garden, 841-867.
[7] Retallack, G. J., 2004. Late Miocene climate and life on land in Oregon within a context of Neogene global change. Palaeogeography, Palaeoclimatology, Palaeoecology, 214(1), 97-123.

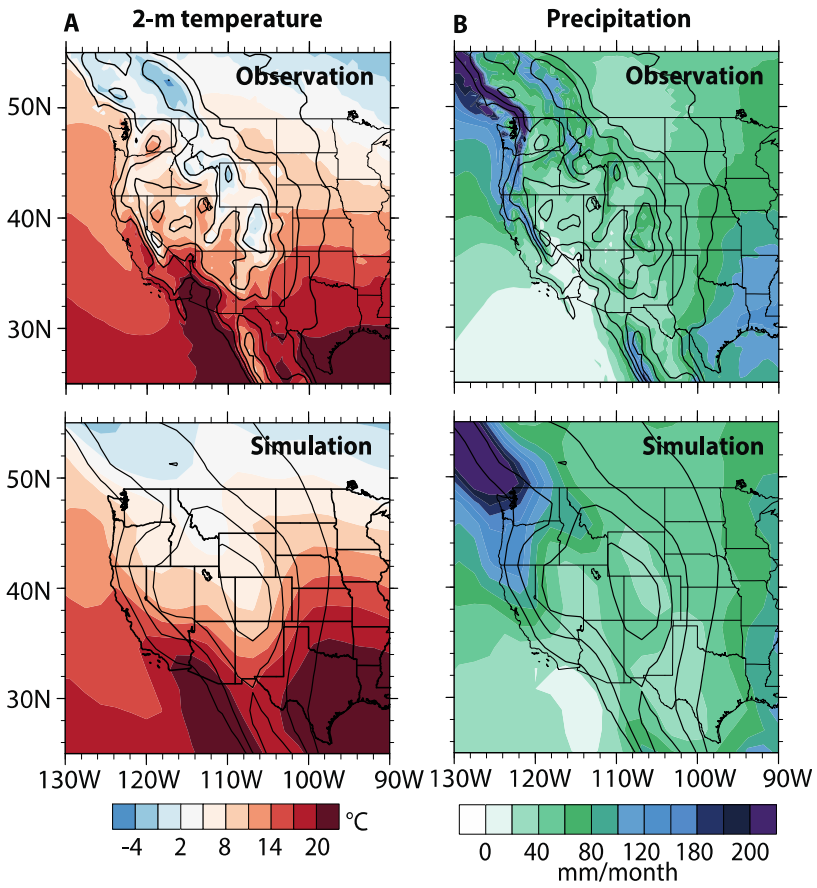


Figure DR1. Comparison of simulated present-day climate with observations. A: mean annual 2-m temperature. B: mean-annual precipitation. Black contours (at 500 m interval starting from 500 m): present-day elevations using 9-point smoothing on 10" GTOPO30 data (upper row) and prescribed modern topography in the model (lower row). The model reproduces observed broad scale patterns of temperature and precipitation, but lacks sufficient horizontal resolution to simulate local variability associated with small-scale topographic gradients.

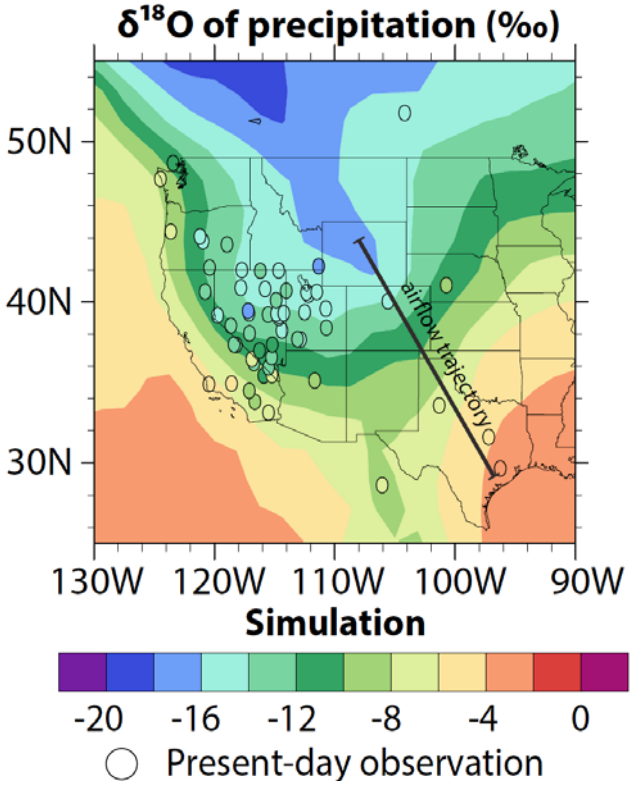


Figure DR2. Comparison of simulated (color shading) and observed $\delta^{18}O$ in precipitation ($\delta^{18}O_p$). Filled circles: observed $\delta^{18}O_p$ from GNIP and USNIP datasets complied by Bowen and Revenaugh, (2003). The thick black line shows the trajectory along which the modern continental $\delta^{18}O_{sw}$ gradient is calculated based on the model simulation.

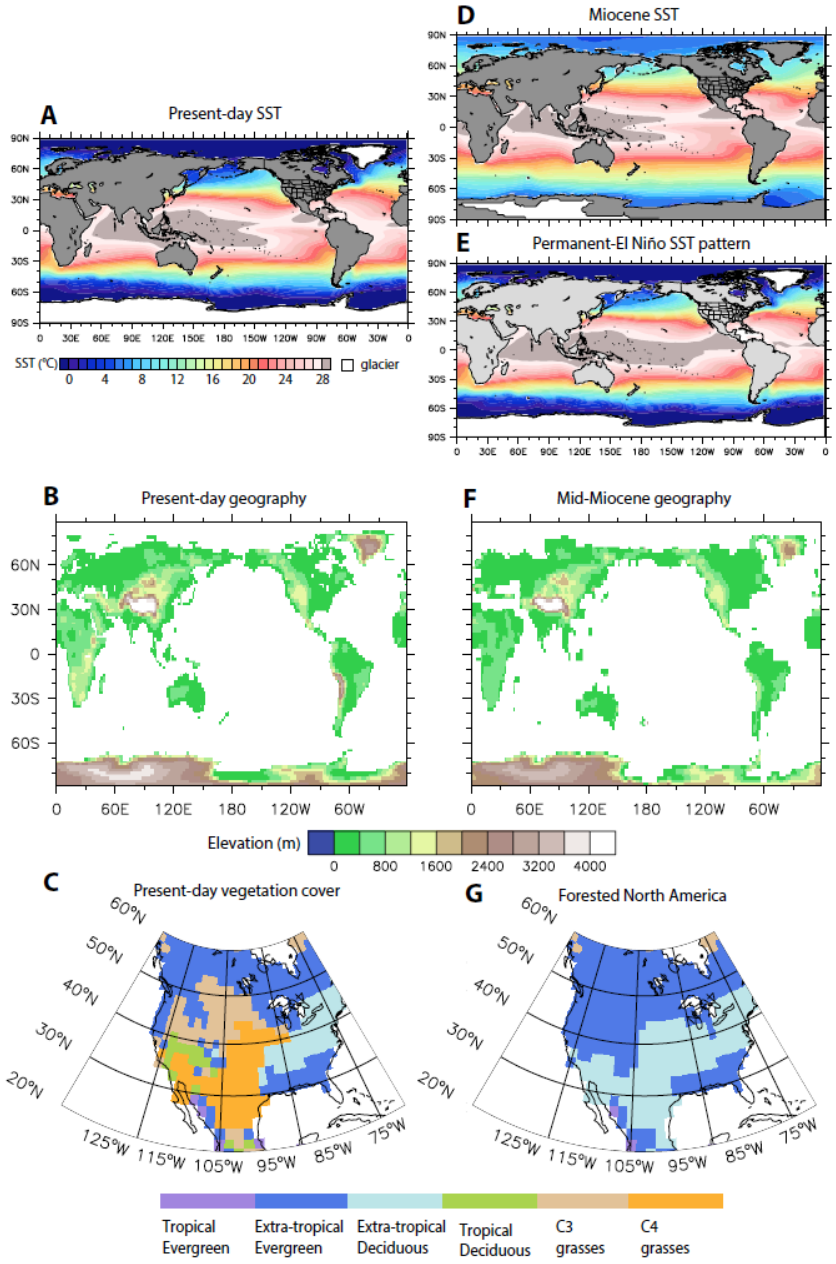


Figure DR3. Prescribed boundary conditions in the model. A-C: present-day global SSTs, geography and North America vegetation cover. D-G: prescribed early Neogene boundary conditions for individual sensitivity experiments featuring steepened equator-to-pole temperatures gradient (D), and tropical Pacific zonal SST gradient (E), early Neogene geographic and topographic configuration (F), and reforestation of North America (G), respectively.

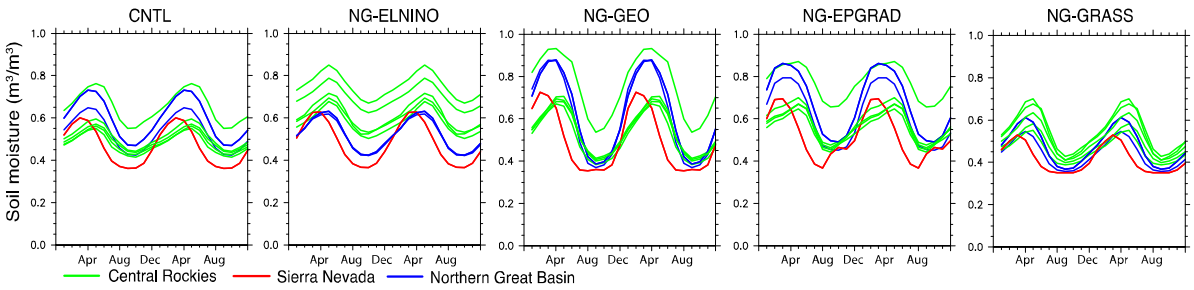


Figure DR4. Seasonal cycle of soil moisture content ($m^3/m^3$) of Neogene proxy sites in different simulations. Experiment IDs are listed in Table DR1. Locations of sites are shown in Figure 1 and listed in Table DR3.

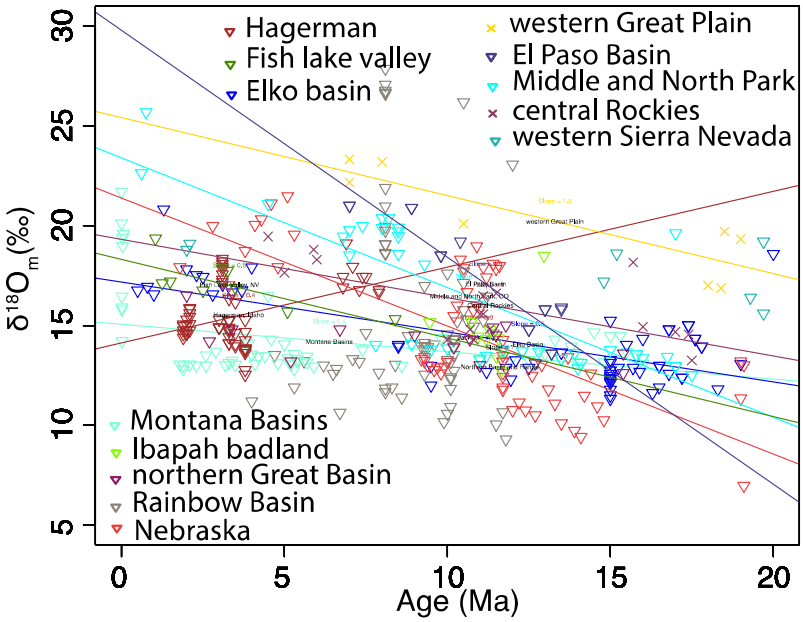


Figure DR5. Overview of published Neogene $\delta^{18}O_m$ records of the western U.S. Corresponding trends are reported in Table DR3.

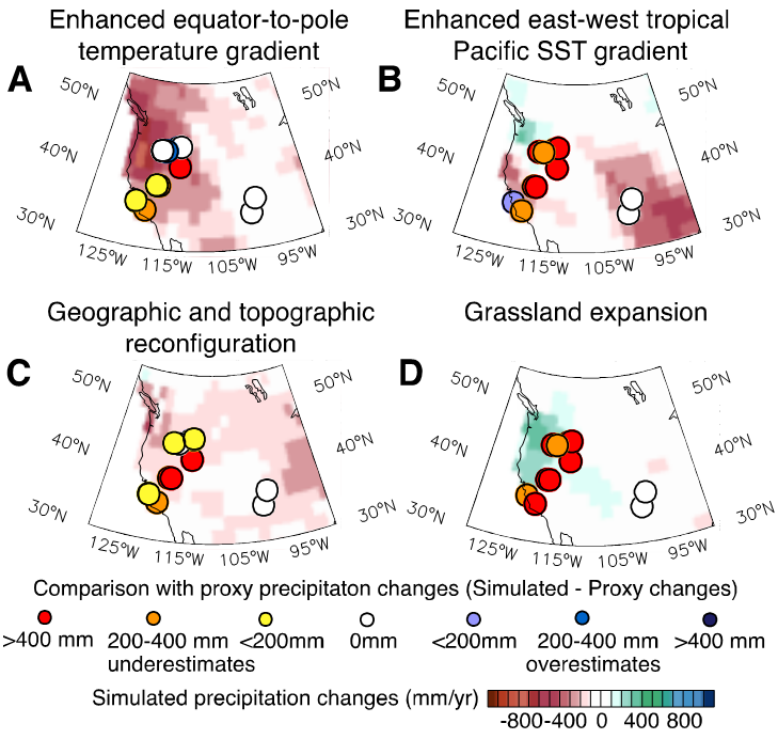


Fig. DR6. Comparison of proxy (filled circles) and simulated Neogene annual precipitation changes (shaded). Reconstructed changes are calculated by subtracting early Neogene proxy estimates (12 – 18 Ma) from present-day observations (1982-2011, MERRA data) at the corresponding proxy sites. Simulated changes are mean annual precipitation differences between control and early Neogene sensitivity cases.

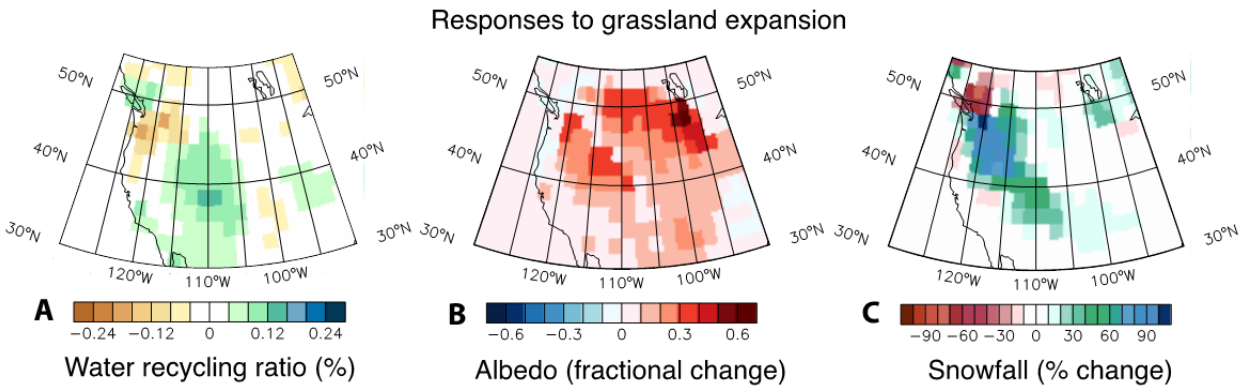


Figure DR7. Simulated climate responses to Neogene grassland expansion. A: fractionation responses of water recycling ratio, defined as the ratio of evapotranspiration versus precipitation. B: fractional responses of surface albedo relative to the albedo of forested western U.S. C: responses of annual total amount of snowfall. Grassland expansion, although increases water recycling ratio, leads to cooling, increase in surface albedo and high altitude snowfall across the western U.S. Consequently, the $\delta^{18}O_{sw}$ responses show melting season depletion and negligible changes of the annual average.

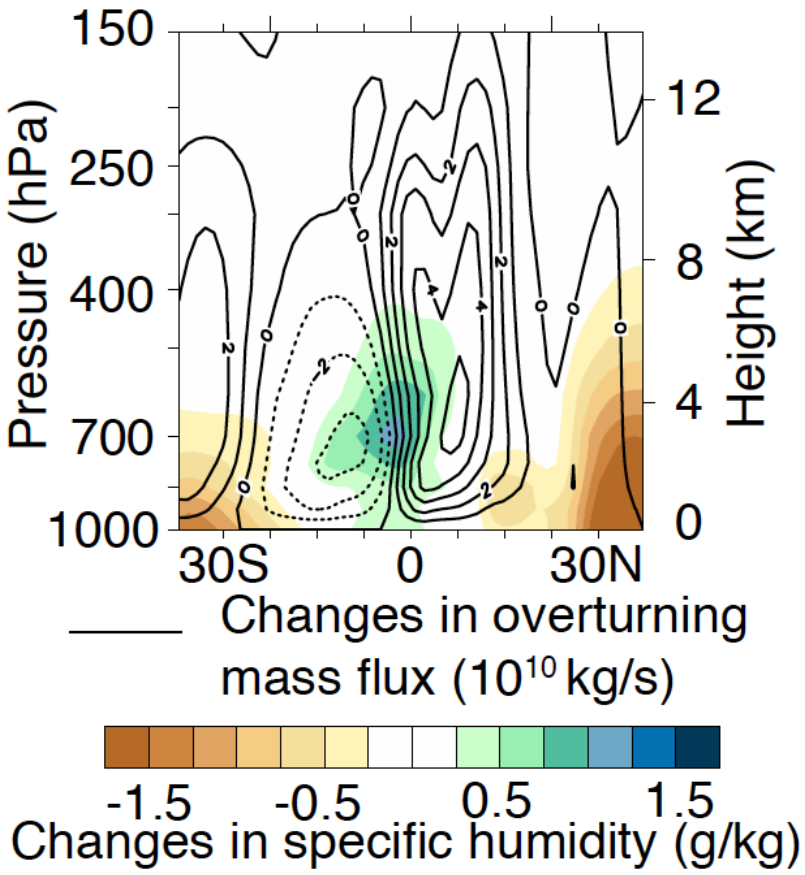


Figure DR8. Responses of zonal-mean overturning mass flux (kg/s, contour) and specific humidity (g/kg, shaded) to Neogene strengthening of EPGRAD.

References

Axelrod D. I., 1979. Desert vegetation, its age and origin. In: Goodin JR & DK Northington (eds). Arid Land Plant Resources: 1-72. International Center for Arid and Semi-arid Land Studies, Texas Tech University, Lubbock, Texas.

Axelrod D. I., 1985. Miocene floras from the Middlegate basin, west-central Nevada. University of California Publications in Geological Sciences 129.

Axelrod D. I., 1991. The Miocene Buffalo Canyon flora, western Nevada. University of California Publications in Geological Sciences 135.

Axelrod D. I., 1995. The middle Miocene Purple Mountain flora of western Nevada: Univ. of California Publ. Geol. Sci., 139, 62 p.

Bowen, G.J., Revenaugh, J., 2003. Interpolating the isotopic composition of modern meteoric precipitation. Water Resources Research 39. doi:10.1029/2003WR002086

Breecker, D.O., Sharp, Z.D., McFadden, L.D., n.d. Seasonal bias in the formation and stable isotopic composition of pedogenic carbonate in modern soils from central New Mexico, USA. Geol Soc America Bull 121, 630–640. doi:10.1130/B26413.1

Friedman I, O'Neil JR. 1977. Compilation of stable isotope fractionation factors of geochemical interest. In USGS Prof. Pap. 440-KK, Data of Geochemistry, ed. M Fleischer, pp. KK1–12. Reston, VA: U.S. Geol. Surv., 6th ed.

Friedman, I., Gleason, J., and Warden, A., 1993, Ancient climate from deuterium content of water in volcanic glass, in Swart, P.K., et al., eds., Climate change in continental isotopic records: American Geophysical Union Geophysical Monograph 78, p. 309–319.

Goldner, A., Herold, N., Huber, M., 2014. The challenge of simulating the warmth of the mid-Miocene climatic optimum in CESM1. Clim. Past 10, 523–536. doi:10.5194/cp-10-523-2014

Herold, N., Huber, M., Muller, R.D., 2011. Modeling the Miocene Climatic Optimum. Part I: Land and Atmosphere*. J. Climate 24, 6353–6372. doi:10.1175/2011JCLI4035.1

Herold, N., Huber, M., Müller, R. D., & Seton, M. 2012. Modeling the Miocene climatic optimum: Ocean circulation. Paleoceanography, *27*(1). doi:10.1029/2010PA002041, 2012

Herold, N., Seton, M., Muller, R.D., You, Y., Huber, M., 2008. Middle Miocene tectonic boundary conditions for use in climate models. Geochemistry, Geophysics, Geosystems 9.

Leopold, E. B., and Denton, M. F., 1987. Comparative age of grassland and steppe east and west of the northern rocky mountain. Annals of the Missouri Botanical Garden, 841-867.

McQuarrie, N., Wernicke, B.P., 2005. An animated tectonic reconstruction of southwestern North America since 36 Ma. Geosphere 1, 147–172. doi:10.1130/GES00016.S1

Molnar, P., Cane, M.A., 2007. Early pliocene (pre-Ice Age) El Nino-like global climate: Which El Nino? Geosphere 3, 337–365. doi:10.1130/GES00103.1

Retallack, G. J., 2004. Late Miocene climate and life on land in Oregon within a context of Neogene global change. Palaeogeography, Palaeoclimatology, Palaeoecology, 214(1), 97-123.

Rienecker, M.M., Suarez, M.J., Gelaro, R., Todling, R., Bacmeister, J., Liu, E., Bosilovich, M.G., Schubert, S.D., Takacs, L., Kim, G.-K., Bloom, S., Chen, J., Collins, D., Conaty, A., da Silva, A., Gu, W., Joiner, J., Koster, R.D., Lucchesi, R., Molod, A., Owens, T., Pawson, S., Pegion, P., Redder, C.R., Reichle, R., Robertson, F.R., Ruddick, A.G., Sienkiewicz, M., Woollen, J., 2011. MERRA: NASA's modern-era retrospective analysis for research and applications. J. Climate 24, 3624–3648.

Sheldon, N. D., 2006. Using paleosols of the Picture Gorge Basalt to reconstruct the middle Miocene climatic optimum. PaleoBios, 26(2), 27-36.

Sheppard S. M. F. and Gilg H. A., 1996. Stable isotope geochemistry of clay minerals. Clay Miner. 31, 1–24.

Smith, T. M., and Reynolds, R. W., 2004. Improved extended reconstruction of SST (1854-1997). Journal of Climate, 17(12), 2466-2477.